MEASUREMENTS OF FLUTTER DERIVATIVES
OF A BRIDGE DECK SECTIONAL MODEL

Leonardo Gunawan, Hadyan Hafizh, Hari Muhammad

Institut Teknologi Bandung
Faculty of Mechanical and Aerospace Engineering
Ganesa 10, Bandung 40132, Indonesia
tel.: +62 22 2504243, fax: +62 22 2534199
e-mail: gun@ae.itb.ac.id, hafizh@alumni.itb.ac.id, harmad@ae.itb.ac.id

Abstract

Aeroelastic phenomena should be considered during the design phase of long span bridges. One of the aeroelastic problems is flutter, the dynamic instability that may cause structural failure at a wind speed called the flutter speed. The prediction of flutter speed of a bridge needs a thorough modelling of bridge stiffness, inertias, and especially its unsteady aerodynamic forces. The potential flow theory is not applicable to calculate unsteady aerodynamics of oscillating bridges due to their non-streamlined complex geometry, and the non-avoidable flow separation. For these reasons, a semi empirical model proposed by Scanlan is used to describe unsteady aerodynamic forces on an oscillating bridge deck. In this model, relation between unsteady aerodynamic forces and motion of the bridge is modelled using parameters known as flutter derivatives. The values of flutter derivatives can be identified from the free vibration responses of an elastic bridge at several wind-speeds. This paper presents wind tunnel tests and flutter derivatives identification of a sectional aeroelastic bridge model. Modified Ibrahim Time Domain method was applied to identify the eigenvalues and eigenvectors of the model at each wind speed, from which the flutter derivatives can be calculated. The results show that the measurement procedure is able produce flutter derivatives, which are in good agreement with those obtained by other researchers.

Keywords: transport, road transport

1. Introduction

Study of bridge aeroelasticity is needed during the design phase of long span bridges. One phenomenon that should be considered is the flutter, an unstable self-excited vibration in which the structure extracts energy from the air stream. Below the critical speed, the motions of the structure are damped out, whereas above the critical speed, the motions are unstable since the damping of the system is negative. This phenomenon can lead to a catastrophic failure, such as the failure of Tacoma Narrows Bridge as shown in Fig. 1 [1, 2].
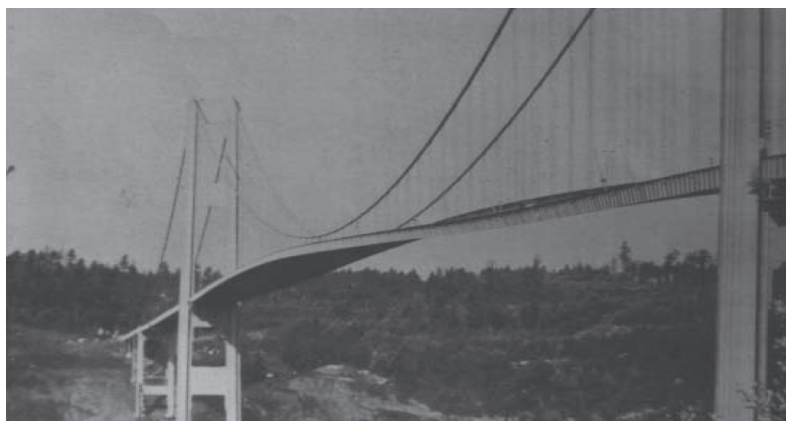

Fig. 1. Flutter of Tacoma Narrow Bridge

Flutter phenomena can be investigated by using analytical, experimental, and numerical methods. For bridge decks with complex geometry, analytical and numerical methods lead to complex mathematical forms. Therefore, predictions of the flutter speed of the bridges should be verified using wind-tunnel tests, either for full bridge model or for partial model of the bridge [3, 4]. For preliminary study, the numerical analysis can be carried out by formulating the unsteady aerodynamic forces using experimental data. This paper presents the measurement of the unsteady aerodynamic coefficients, or the flutter derivatives, of a bridge deck sectional model.

2. Theory

2.1. Bridge Aeroelastic Model

Figure 2 shows a model of an oscillating bridge sectional model in wind stream with c.g. at the middle position. The model is supported by linear and torsional spring, k_h and k_α. The equation of motion of the model in the vertical and rotational motion, $h(t)$ and $\alpha(t)$ respectively is:

$$\begin{bmatrix} m & 0 \\ 0 & I \end{bmatrix} \begin{Bmatrix} \ddot{h} \\ \ddot{\alpha} \end{Bmatrix} + \begin{bmatrix} c_h & 0 \\ 0 & c_\alpha \end{bmatrix} \begin{Bmatrix} \dot{h} \\ \dot{\alpha} \end{Bmatrix} + \begin{bmatrix} k_h & 0 \\ 0 & k_\alpha \end{bmatrix} \begin{Bmatrix} h \\ \alpha \end{Bmatrix} = \begin{Bmatrix} L \\ M_\alpha \end{Bmatrix}, \tag{1}$$

where L, M_α are the aerodynamic force and moment working on the bridge deck. In aeroelastic instability analysis, only motion dependent aerodynamic forces are considered. The aerodynamic force and moment can be related to the motion of the bridge as follow [5]:

$$L = \frac{1}{2}\rho U^2 B \left[KH_1^*(K)\frac{\dot{h}}{U} + KH_2^*(K)\frac{B\dot{\alpha}}{U} + K^2 H_3^*(K)\alpha + K^2 H_4^*(K)\frac{h}{B} \right],$$

$$M = \frac{1}{2}\rho U^2 B^2 \left[KA_1^*(K)\frac{\dot{h}}{U} + KA_2^*(K)\frac{B\dot{\alpha}}{U} + K^2 A_3^*(K)\alpha + K^2 A_4^*(K)\frac{h}{B} \right], \tag{2}$$

where: ρ – air density, U – mean wind velocity, B – chord, ω – frequency, $K = B\omega/U$ – reduced frequency and $H_i^*(K), A_i^*(K), i = 1,...,4$: flutter derivatives. The flutter derivatives of a body that represents a thin plate can be obtained from the formula developed by Theodorsen [6]. For a bluff body, they are obtained from wind tunnel tests.
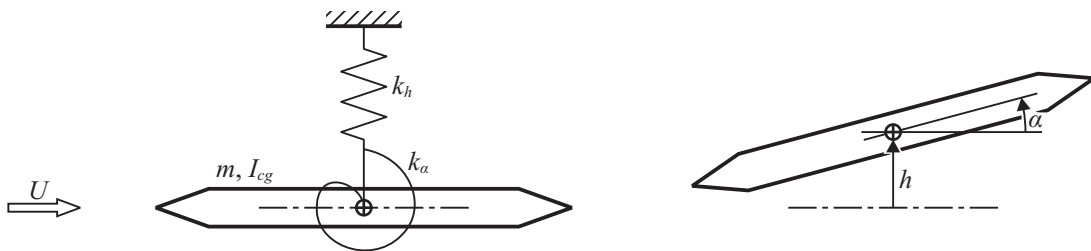

Fig. 2. Bridge deck sectional model and its displacement

By substituting Eq. (2) into Eq. (1), and mathematically manipulating the result, a normalized aeroelastic equation of motion of the bridge model can be obtained:

$$\mathbf{I\ddot{x}} + \mathbf{C}^{eff}\mathbf{\dot{x}} + \mathbf{K}^{eff}\mathbf{x} = \mathbf{0}, \tag{3}$$

where:

$$\mathbf{I} = \begin{bmatrix} 1 & 0 \\ 0 & 1 \end{bmatrix},$$

$$\mathbf{C}^{eff} = \begin{bmatrix} 2\zeta_h\omega_h - \dfrac{\rho B^2\omega_h}{2m}H_1^* & -\dfrac{\rho B^3\omega_\alpha}{2m}H_2^* \\[2ex] -\dfrac{\rho B^3\omega_h}{2I}A_1^* & 2\zeta_\alpha\omega_\alpha - \dfrac{\rho B^4\omega_\alpha}{2I}A_2^* \end{bmatrix},$$

$$\mathbf{K}^{eff} = \begin{bmatrix} \omega_h^2 - \dfrac{\rho B^2\omega_h^2}{2m}H_4^* & -\dfrac{\rho B^3\omega_\alpha^2}{2m}H_3^* \\[2ex] -\dfrac{\rho B^3\omega_h^2}{2I}A_4^* & \omega_\alpha^2 - \dfrac{\rho B^4\omega_\alpha^2}{2I}A_3^* \end{bmatrix},$$

$$\mathbf{x} = [h \quad \alpha]^T,$$

$$\omega_h = \sqrt{k_h/m},$$

$$\omega_\alpha = \sqrt{k_\alpha/I_{cg}}.$$

The parameters of the aeroelastic model can experimentally be determined. First, its free vibration responses at several wind speeds (including zero) are measured, from which the frequencies, dampings, and mode shapes of the model are identified. Then, the $\mathbf{C}^{eff}$ and $\mathbf{K}^{eff}$ matrices are reconstructed. The flutter derivatives at a wind speed are calculated from the difference between $\mathbf{C}^{eff}$ and $\mathbf{K}^{eff}$ at the wind speed to those without wind by as follow:

$$H_1^*(K) = -2m(C_{11}^{eff} - C_{11}^0)/(\rho B^2\omega_h),$$

$$H_2^*(K) = -2m(C_{12}^{eff} - C_{12}^0)/(\rho B^3\omega_\alpha),$$

$$H_3^*(K) = -2m(K_{12}^{eff} - K_{12}^0)/(\rho B^3\omega_\alpha^2),$$

$$H_4^*(K) = -2m(K_{11}^{eff} - K_{11}^0)/(\rho B^2\omega_h^2),$$

$$A_1^*(K) = -2I(C_{21}^{eff} - C_{21}^0)/(\rho B^3\omega_h),$$

$$A_2^*(K) = -2I(C_{22}^{eff} - C_{22}^0)/(\rho B^4\omega_\alpha),$$

$$A_3^*(K) = -2I(K_{22}^{eff} - K_{22}^0)/(\rho B^4\omega_\alpha^2),$$

$$A_4^*(K) = -2I(K_{21}^{eff} - K_{21}^0)/(\rho B^3\omega_h^2).$$

$$(4)$$

2.2 Identification of model dynamic characteristics

The eigenvalues and eigenvectors of the model are identified from its free vibration response by using Modified Ibrahim Time Domain (MITD) method [7, 8], which is a recursive procedure based on the Ibrahim Time Domain (ITD) method [9].

ITD Method

Figure 3 illustrates the measured free vibrations data in the form of the vertical and the rotational displacements sampled with a time step Δt. Theoretically, the free vibration response can be modelled as the superposition of vibrations at two frequencies, each at its mode shape:

$$\mathbf{x}(t) = [h(t) \ \alpha(t)]^T = \sum_{m=1}^{4} \beta_m p_m e^{\lambda_m t}, \qquad (5)$$

where:
β_m – constants to satisfy the initial conditions,
p_m – vibration mode shapes,
$\lambda_m = a_m + ib_m = \zeta_m\omega_m + i\omega_m\sqrt{1-\zeta_m^2}$ – complex natural frequencies, $\lambda_2 = \lambda_1^*$, $\lambda_4 = \lambda_3^*$.
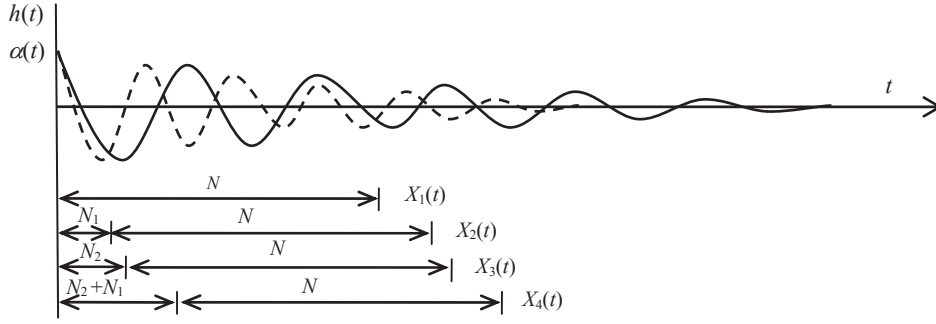
Fig. 3. Measured data and data sets for identification

For ITD method, four data sets of equal size are obtained from the measured data, as illustrated in Fig. 3. The first data set contains N data points, the second data set is obtained by shifting first data set to the right by N_1, the third and fourth data sets are obtained by shifting the first and second data to the right by N_2. The shift factors N_1 and N_2 are determined by following Sarkar [7]:

$$N_1 = 1/(4\Delta t\, f_d), \quad N_2 = N_1 \pm 1 \text{ or } 2, \tag{6}$$

where f_d is the highest frequency of the system.

The procedure described previously provides 4 data sets as follow:

$$\mathbf{X}_1 = \begin{bmatrix} h(1) & \dots & h(N) \\ \alpha(1) & \dots & \alpha(N) \end{bmatrix},$$

$$\mathbf{X}_2 = \begin{bmatrix} h(1+N) & \dots & h(N+N_1) \\ \alpha(1+N) & \dots & \alpha(N+N_1) \end{bmatrix},$$

$$\mathbf{X}_3 = \begin{bmatrix} h(1+N_2) & \dots & h(N+N_2) \\ \alpha(1+N_2) & \dots & \alpha(N+N_2) \end{bmatrix}, \tag{7}$$

$$\mathbf{X}_4 = \begin{bmatrix} h(1+N_1+N_2) & \dots & h(N+N_1+N_2) \\ \alpha(1+N_1+N_2) & \dots & \alpha(N+N_1+N_2) \end{bmatrix}.$$

Following Eq. (5), each data set can be modelled as:

$$\mathbf{X}_1 = \mathbf{P}\mathbf{\Lambda}_1; \quad \mathbf{X}_2 = \mathbf{P}\mathbf{\Lambda}_2; \quad \mathbf{X}_3 = \mathbf{P}\mathbf{\Lambda}_3; \quad \mathbf{X}_4 = \mathbf{P}\mathbf{\Lambda}_4, \tag{8}$$

where:

$$\mathbf{P} = \begin{bmatrix} \beta_1 p_{11} & \beta_2 p_{11} & \beta_3 p_{21} & \beta_4 p_{21} \\ \beta_1 p_{12} & \beta_2 p_{12} & \beta_3 p_{22} & \beta_4 p_{22} \end{bmatrix} - 2\times 4 \text{ modal matrix,}$$

$$\mathbf{\Lambda}_1 = \begin{bmatrix} e^0 & \dots & e^{\lambda_1(N-1)\Delta t} \\ \vdots & \ddots & \vdots \\ e^0 & \dots & e^{\lambda_4(N-1)\Delta t} \end{bmatrix} - 4\times N \text{ spectral matrix of the system,}$$

$$\mathbf{\Lambda}_2 = \begin{bmatrix} e^{\lambda_1 N_1 \Delta t} & \dots & e^{\lambda_1(N+N_1-1)\Delta t} \\ \vdots & \ddots & \vdots \\ e^{\lambda_4 N_1 \Delta t} & \dots & e^{\lambda_4(N+N_1-1)\Delta t} \end{bmatrix} = \begin{bmatrix} e^{\lambda_1 N_1 \Delta t} & 0 & 0 \\ 0 & \ddots & 0 \\ 0 & 0 & e^{\lambda_4 N_1 \Delta t} \end{bmatrix} \begin{bmatrix} e^0 & \dots & e^{\lambda_1(N-1)\Delta t} \\ \vdots & \ddots & \vdots \\ e^0 & \dots & e^{\lambda_4(N-1)\Delta t} \end{bmatrix} = \mathbf{\Delta}_{N_1}\mathbf{\Lambda}_1,$$

$$\mathbf{\Lambda}_3 = \begin{bmatrix} e^{\lambda_1 N_2 \Delta t} & \dots & e^{\lambda_1(N_2+N-1)\Delta t} \\ \vdots & \ddots & \vdots \\ e^{\lambda_4 N_2 \Delta t} & \dots & e^{\lambda_4(N_2+N-1)\Delta t} \end{bmatrix} = \begin{bmatrix} e^{\lambda_1 N_2 \Delta t} & 0 & e^{\lambda_1 N_2 \Delta t} \\ 0 & \ddots & 0 \\ 0 & 0 & e^{\lambda_4 N_2 \Delta t} \end{bmatrix} \begin{bmatrix} e^0 & \dots & e^{\lambda_1(N-1)\Delta t} \\ \vdots & \ddots & \vdots \\ e^0 & \dots & e^{\lambda_4(N-1)\Delta t} \end{bmatrix} = \mathbf{\Delta}_{N_2}\mathbf{\Lambda}_1,$$

$$\mathbf{\Lambda}_4 = \begin{bmatrix} e^{\lambda_1(N_2+N_1)\Delta t} & \dots & e^{\lambda_1(N_2+N_1+N-1)\Delta t} \\ \vdots & \ddots & \vdots \\ e^{\lambda_4(N_2+N_1)\Delta t} & \dots & e^{\lambda_4(N_2+N_1+N-1)\Delta t} \end{bmatrix} = \begin{bmatrix} e^{\lambda_1(N_1+N_1)\Delta t} & 0 & 0 \\ 0 & \ddots & 0 \\ 0 & 0 & e^{\lambda_4(N_1+N_1)\Delta t} \end{bmatrix} \begin{bmatrix} e^0 & \dots & e^{\lambda_1(N-1)\Delta t} \\ \vdots & \ddots & \vdots \\ e^0 & \dots & e^{\lambda_4(N-1)\Delta t} \end{bmatrix} = \mathbf{\Delta}_{N_1}\mathbf{\Delta}_{N_2}\mathbf{\Lambda}_1.$$

By using the relation between the spectral matrices, Eq. (8) can be written as:

$$\begin{aligned} \mathbf{X}_1 &= \mathbf{P}\mathbf{\Lambda}_1, \\ \mathbf{X}_2 &= \mathbf{P}\mathbf{\Lambda}_2 = \mathbf{P}\mathbf{\Delta}_{N_1}\mathbf{\Lambda}_1 = \mathbf{Q}\mathbf{\Lambda}_1, \\ \mathbf{X}_3 &= \mathbf{P}\mathbf{\Lambda}_3 = \mathbf{P}\mathbf{\Delta}_{N_2}\mathbf{\Lambda}_1, \\ \mathbf{X}_4 &= \mathbf{P}\mathbf{\Lambda}_4 = \mathbf{P}\mathbf{\Delta}_{N_1}\mathbf{\Delta}_{N_2}\mathbf{\Lambda}_1 = \mathbf{Q}\mathbf{\Delta}_{N_2}\mathbf{\Lambda}_1. \end{aligned} \tag{9}$$

Data sets $\mathbf{X}_1$ and $\mathbf{X}_2$ can be combined as a single equation, and also the data sets $\mathbf{X}_3$ and $\mathbf{X}_4$:

$$\begin{bmatrix} \mathbf{X}_1 \\ \mathbf{X}_2 \end{bmatrix} = \begin{bmatrix} \mathbf{P} \\ \mathbf{Q} \end{bmatrix}\mathbf{\Lambda}_1 \quad \text{and} \quad \begin{bmatrix} \mathbf{X}_3 \\ \mathbf{X}_4 \end{bmatrix} = \begin{bmatrix} \mathbf{P} \\ \mathbf{Q} \end{bmatrix}\mathbf{\Delta}_{N_2}\mathbf{\Lambda}_1. \tag{10}$$

By substituting $\mathbf{\Lambda}_1$ obtained from the first combination into the second one, and after some mathematical manipulation, an eigenvalues problem is obtained:

$$\left[\begin{bmatrix} \mathbf{X}_1 \\ \mathbf{X}_2 \end{bmatrix}^{-1}\begin{bmatrix} \mathbf{X}_3 \\ \mathbf{X}_4 \end{bmatrix}\right]\begin{bmatrix} \mathbf{P} \\ \mathbf{Q} \end{bmatrix} = \mathbf{\Delta}_{N_2}\begin{bmatrix} \mathbf{P} \\ \mathbf{Q} \end{bmatrix} \quad \text{or} \quad \mathbf{A}\mathbf{\Psi} = \mathbf{\Psi}\mathbf{\Delta}_{N_2}, \tag{11}$$

where $\mathbf{A} = \mathbf{Z}^{-1}\hat{\mathbf{Z}}$, $\mathbf{Z} = [\mathbf{X}_1 \quad \mathbf{X}_2]^T$, $\hat{\mathbf{Z}} = [\mathbf{X}_3 \quad \mathbf{X}_4]^T$ and $\mathbf{\Psi} = [\mathbf{P} \quad \mathbf{Q}]^T$.

Solutions of Eq.(11) are eigenvectors and eigenvalues matrices, $\mathbf{\Psi}$ and $\mathbf{\Delta}_{N_2}$. The complex mode shape matrix $\mathbf{P}$ is the upper half of $\mathbf{\Psi}$. By assuming that the mth eigenvalue is in the form of $\Delta_{N_2 m} = \alpha_m + \beta_m$, the damping factor and the damped natural frequency of Eq. (5) can be calculated as:

$$a_m = \zeta_m\omega_m = -\ln(\alpha_m^2 + \beta_m^2)/(2N_2\Delta t) \quad \text{and} \quad b_m = \omega_m\sqrt{1-\zeta_m^2} = \tan^{-1}(\beta_m/\alpha_m)/(N_2\Delta t). \tag{12}$$

When $\mathbf{Z}$ and $\hat{\mathbf{Z}}$ in Eq.(11) are non-square matrices, the inverse procedure leads to the pseudo-inverse technique and gives the least squares equivalent in two forms which are known as a positive shift $\mathbf{A}^+ = (\hat{\mathbf{Z}}\hat{\mathbf{Z}}^T)(\mathbf{Z}\hat{\mathbf{Z}}^T)^{-1}]$ and a negative time shift $\mathbf{A}^- = (\hat{\mathbf{Z}}\mathbf{Z}^T)(\mathbf{Z}\mathbf{Z}^T)^{-1}]$. A better estimation of the damping factor can be obtained by averaging both equations, i.e. $\mathbf{A} = \frac{1}{2}(\mathbf{A}^+ + \mathbf{A}^-)$.

MITD Method

By using the parameters obtained from ITD method, responses of bridge deck $\overline{\mathbf{X}} = [\overline{h}(t) \quad \overline{\alpha}(t)]^T$ can be simulated according to Eq.(5). Following the data preparation procedure in ITD method, 4 data sets can be built from the simulation results, which can be combined into two variables:

$$\overline{\mathbf{Z}} = \begin{bmatrix} \overline{h}(1) & \dots & \overline{h}(N) \\ \overline{\alpha}(1) & \dots & \overline{\alpha}(N) \\ \overline{h}(1+N_1) & \dots & \overline{h}(N+N_1) \\ \overline{\alpha}(1+N_1) & \dots & \overline{\alpha}(N+N_1) \end{bmatrix} \text{ and } \hat{\overline{\mathbf{Z}}} = \begin{bmatrix} \overline{h}(N_2+1) & \dots & \overline{h}(N_2+N) \\ \overline{\alpha}(N_2+1) & \dots & \overline{\alpha}(N_2+N) \\ \overline{h}(N_2+N_1+1) & \dots & \overline{h}(N_2+N_1+N) \\ \overline{\alpha}(N_2+N_1+1) & \dots & \overline{\alpha}(N_2+N_1+N) \end{bmatrix}. \tag{13}$$

By combining experimental and simulation data, the $\mathbf{A}$ matrix can be built using average scheme:

$$\mathbf{A} = \frac{1}{2}(\mathbf{A}^+ + \mathbf{A}^-) = \frac{1}{2}[(\hat{\overline{\mathbf{Z}}}\hat{\overline{\mathbf{Z}}}^T)(\mathbf{Z}\hat{\overline{\mathbf{Z}}}^T)^{-1} + (\hat{\overline{\mathbf{Z}}}\overline{\mathbf{Z}}^T)(\mathbf{Z}\overline{\mathbf{Z}}^T)^{-1}]. \tag{14}$$

The results of eigenvalue analysis can be used to simulate response of the system. The identification procedure by using the combination of the measured and simulated response is repeated until the eigenvalues and eigenvectors are convergent.

2.3. Reconstruction of $\mathbf{K}^{eff}$ and $\mathbf{C}^{eff}$

The responses simulated from the identification results can be written in state space model:

$$\dot{\mathbf{y}} = \mathbf{G}\mathbf{y}, \tag{15}$$

where $\mathbf{y} = [\mathbf{x}^T \ \dot{\mathbf{x}}^T]^T = [h(t) \ \alpha(t) \ \dot{h}(t) \ \dot{\alpha}(t)]^T$ and $\mathbf{G} = \begin{bmatrix} \mathbf{0} & \mathbf{I} \\ -\mathbf{K}^{eff} & -\mathbf{C}^{eff} \end{bmatrix}$.

With $\mathbf{0}$ – 2×2 zero matrix, $\mathbf{I}$ – 2×2 identity matrix, $\mathbf{C}^{eff}$ and $\mathbf{K}^{eff}$ – the effective damping and stiffness matrices described in Eq. (3). Solution of Eq.(15) can be written as:

$$y(t) = \sum_{m=1}^{4} (\beta_m v_m e^{\lambda_m t}). \tag{16}$$

By comparing equation (16) with equation (5), the mth eigenvector is given by:

$$v_m = \begin{Bmatrix} p_m \\ \lambda_m p_m \end{Bmatrix}. \tag{17}$$

The modal matrix in state-space domain can be expressed as:

$$\mathbf{V} = [v_1, \cdots, v_{2m}] = \begin{bmatrix} \mathbf{P} \\ \mathbf{P}\mathbf{\Lambda} \end{bmatrix}. \tag{18}$$

Therefore, the state matrix can be calculated from the modal matrix in state-space domain:

$$\mathbf{G} = \begin{bmatrix} \mathbf{G}(1,1) & \mathbf{G}(1,2) \\ \mathbf{G}(2,1) & \mathbf{G}(2,2) \end{bmatrix} = \mathbf{V}\mathbf{\Lambda}\mathbf{V}^{-1}. \tag{19}$$

Hence, the effective damping and stiffness of the system are:

$$\mathbf{K}^{eff} = -\mathbf{G}(2,1) \quad \text{and} \quad \mathbf{C}^{eff} = -\mathbf{G}(2,2). \tag{20}$$

3. Experiment Procedure

The experiment was carried out in the aeroelastic wind tunnel, at the Dept.of Aeronautics and Astronautics of ITB, with test section length of 1180 mm and cross section of 400 mm×400 mm. The model has a span of 350 mm, chord length of 300 mm, and thickness of 25 mm. The model was suspended in the test section with practically 8 identical springs as shown in Fig. 4 [9]. The stiffness of each spring was selected by considering the vertical natural frequency. The chord-wise distance between springs were adjusted by considering the rotational natural frequency. Frequency tuning of the model was also performed by symmetrically adding 4 identical masses inside the model, and adjusting their chord-wise distance. The vertical and rotational natural frequency of the model are 4.5 Hz and 6.5 Hz, respectively.

Two B&K 4371 accelerometers were installed inside the model to measure the front and aft responses at mid span position. The B&K 2525 conditioning amplifiers integrated the acceleration signals twice into the displacement signals. A data acquisition system sampled the data at rate of 1000 Hz. The two displacement signals were then filtered and manipulated into vertical and rotational motion of the bridge at its c.g. Measurement of bridge response due to an initial displacement disturbance were carried out at 18 wind speeds from 0 m/s to 10 m/s. At each wind speed, three measurements were carried out.

From the data of vertical and rotational motion of the bridge, the eigenvalues and eigenvectors of the model at each wind-speed were identified by using MITD method. The effectiveness of the MITD method can be seen in Fig. 5, where simulation of the displacement signal using results of this method are very close to the measured data than that of ITD.
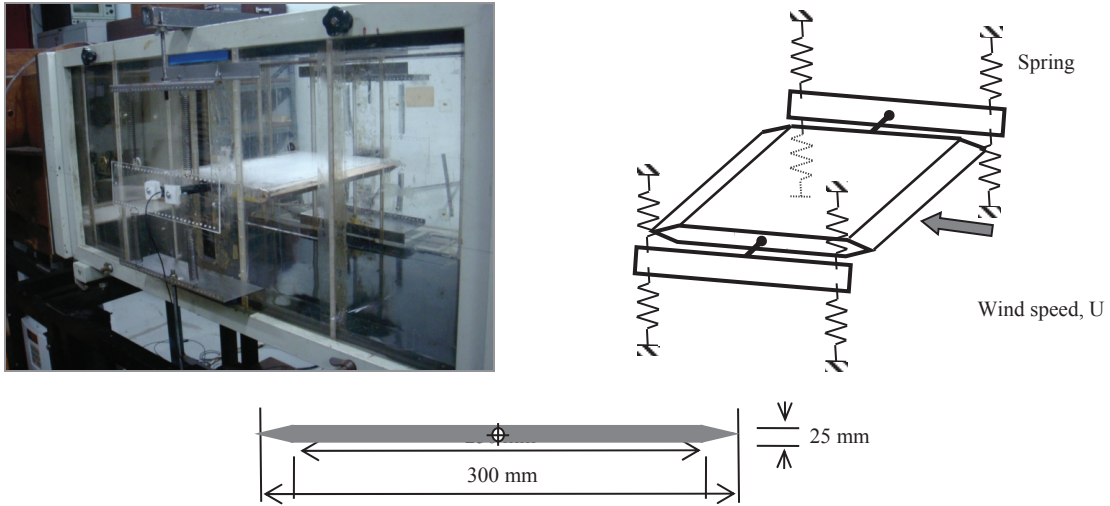
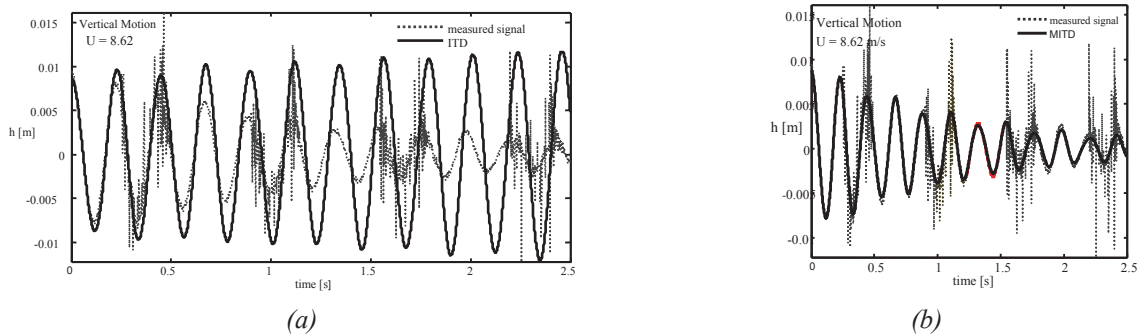Fig. 4. Test setup and deck sectional model

Fig. 5. Simulations of measured vertical displacement data using (a) ITD method (b) MITD method

After the eigenvalues and eigenvectors of the system at each wind speed were identified, the effective stiffness and damping matrix of the model then were calculated using Eq. (17)-(20). Finally, the flutter derivatives were determined by using Eq. (4).

4. Results and Analysis

The identification procedure was applied to the displacement signals at each wind speed. The real and imaginer part of the eigenvalues, which correspond to the damping and the damped natural frequencies are presented in Fig. 6. From three measurements at each wind speed, the identified natural frequencies are practically similar, but the dampings are rather scattered especially at higher wind speeds. The average of the real and imaginer parts of the eigenvalues are shown in Fig. 6 as solid and dashed lines for the rotational and vertical motion. It can be seen that with increasing wind speed, the rotational and vertical natural frequency become closer. The vertical motion damping increases with increasing wind speed, however, the rotational motion damping increases up to about 7.5 m/s and then it decreases. This is the typical characteristic of an aeroelastic system with unstable rotational mode.

From the eigenvalues and eigenvectors of the system, the effective stiffness and damping matrices were reconstructed and flutter derivatives were determined. The results are shown in Fig. 7, where they are compared to theoretical flutter derivatives of a flat plate of similar planform size. It can be seen that at lower wind speeds the measured H_1^*, H_2^*, and H_3^* are similar to those of the thin plate, while at higher speeds their values are different from but their trends are similar to those of the thin plate. The measured H_4^* has different values and trend from that of the thin plate for all wind speeds.
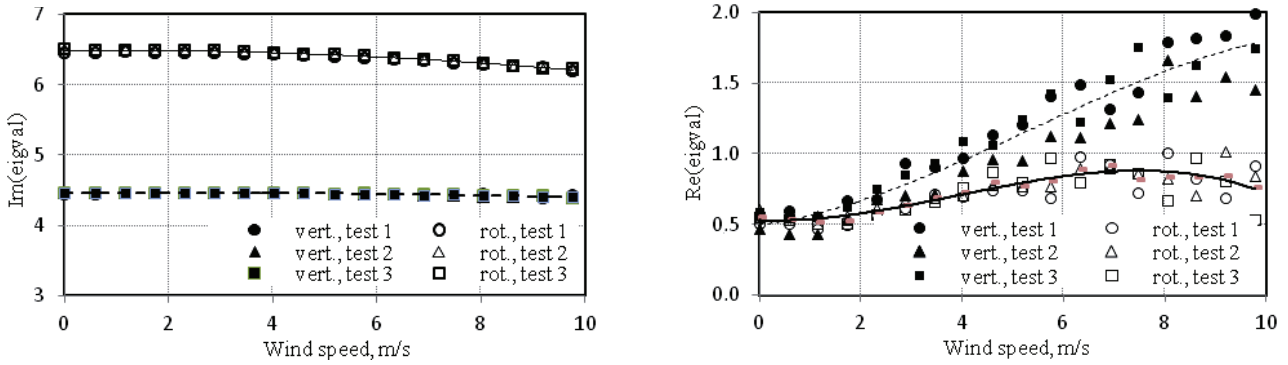
Fig. 6. Imaginer and real eigenvalues (natural frequency and damping) of the model from the three measurements. The averaged data is shown in solid line for rotational motion and dashed line for vertical motion
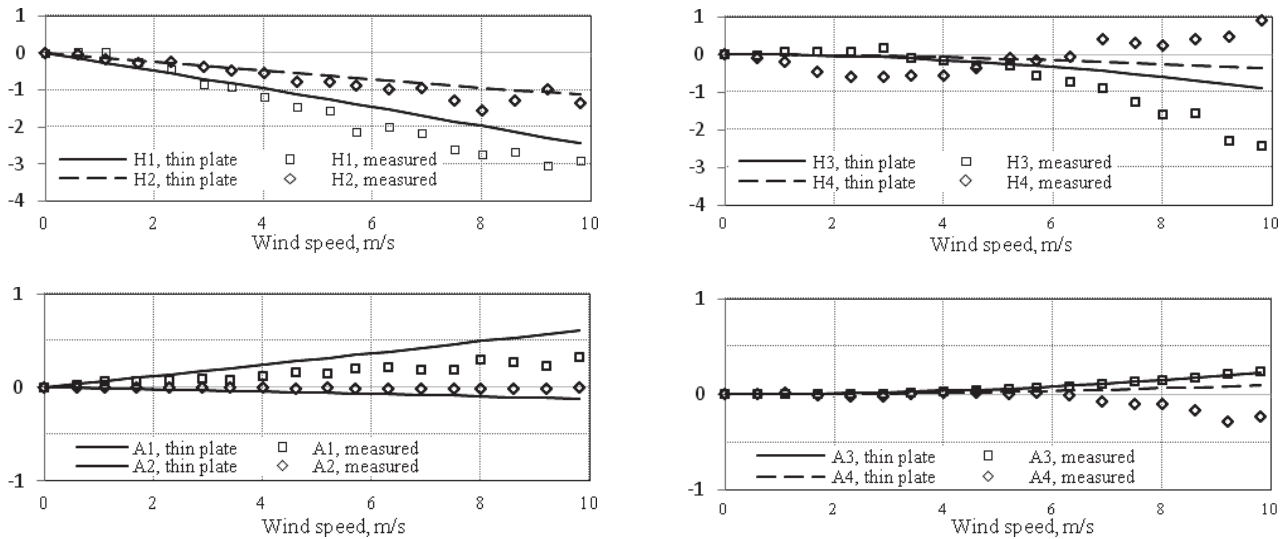

Fig. 7. H^* and A^* derivatives of the bridge model at several wind speeds

The H_4^* is related to the changes in K_{11} or to changes in vertical frequency (Eq. 3 and Eq. 4). Fig. 6 shows that vertical frequencies change only slightly compared to the torsional frequencies. Hence the determination of H_4^* is sensitive to the error in the measurement. Gu [10] also had similar results and pointed out that identification of H_4^* is difficult and very sensitive to noise.

Figure 7 shows that at lower wind speeds the measured A^* derivatives are similar to those of a thin plate. At higher wind speeds, compared to flutter derivatives of a the thin plate, the values of the measured A^* are different but the trends are similar. Except for the A_4^* that has different values and trend from that of the thin plate.

The results are also compared to results of Li [11] who identified the flutter derivatives using the Weighting Ensemble Least-Squares method (WELS). The model tested by Liu has a similar cross section but different mechanical and geometrical parameters. Therefore the flutter derivatives are presented as the function of reduced velocity, $U/(f B)$, as shown in Fig. 8 and Fig. 9. It can be seen that current results are in good agreements with those of Li, especially at low reduced velocity. At high reduced velocity, the measured H_4^* and H_4^* are different from those of Li.

5. Conclusions

Measurement of the flutter derivatives to a bridge section model provides results that are in good agreements with theoretical flutter derivatives of thin plate, especially at low wind speeds. At higher speeds the agreement is less, however, the trends between the measured data and the theoretical values is the same, except for the measured H_4^* and H_4^*.
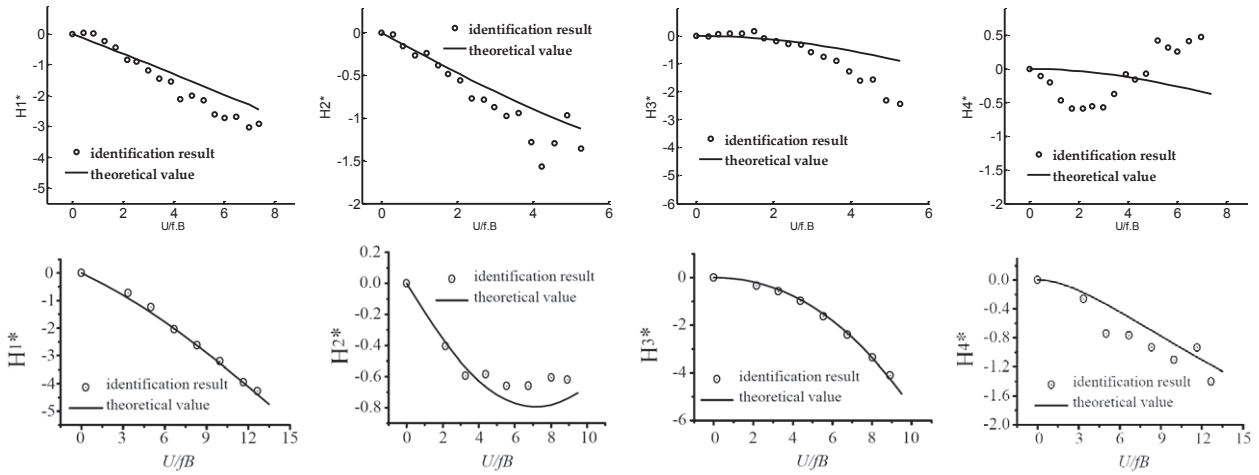
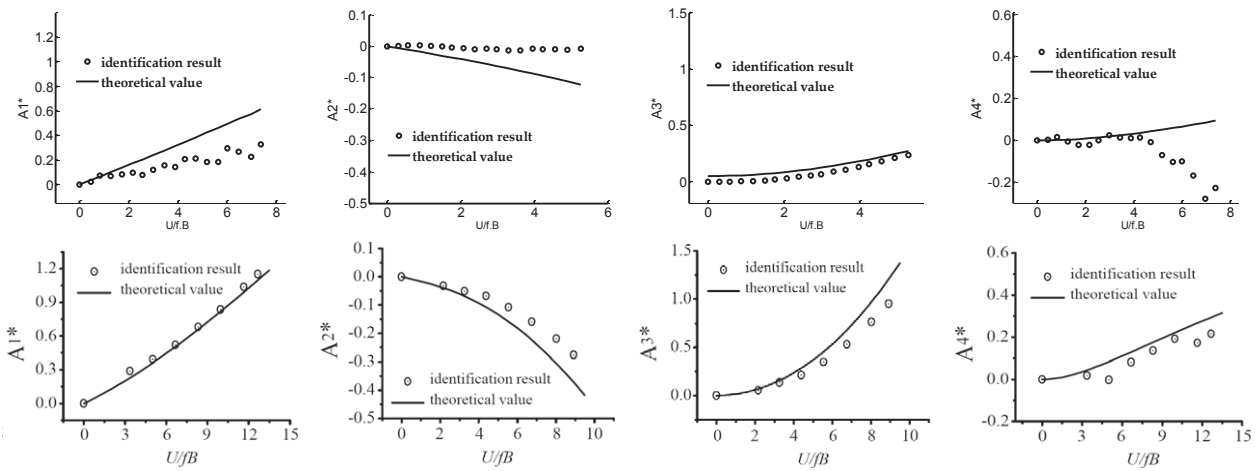*Fig. 8. Comparison of measured H* derivatives (upper row) with those measured by Li [11] (lower row)*

Fig. 9. Comparison of measured A* derivatives (upper row) with those measured by Li [11] (lower row)

The measurement procedure can be used to obtain flutter derivatives of bridge sectional model of other geometries, but the test setup should be improved to get better results at high wind speeds.

References

[1]   Koughan, J., *The Collapse of the Tacoma Narrows Bridge, Evaluation of Competing Theories of Its Demise, and the Effects of the Disaster of Succeeding Bridge Designs*, The Univ. of Texas at Austin, Uniteed States 1996.

[2]   Billah, K. Y., Scanlan, R. H., *Resonance, Tacoma Narrows Bridge Failure, and Under-Graduate Physics Textbooks*, American Journal of Physics, Vol. 59, pp. 118-124, 1991.

[3]   Gunawan, L., Sangaji, S., *Experimental Aeroelastic Study of a Cable Stayed Bridge*, Proc. Experimental & Theoretical Mechanic 2002, Sanur, Bali, Indonesia 2002.

[4]   Fariduzzaman, *Geometry and Wind Turbulence Effects on Vortex Induced Vibration of Long Span Bridge Deck,* Ph.D. Dissertation, Dept. of Aero- and Astronautics, Institut Teknologi Bandung, Indonesia 2007.

[5]   Scanlan, R. H., Tomko, J. J., *Airfoil and Bridge Deck Flutter Derivatives*, Journal of the Engineering Mechanics Division, Vol. 97 (EM 6), pp. 1717-1737, 1971.

[6]   Theodorsen, T., *General Theory of Aero-dynamic Instability and The Mechanism of Flutter*, NACA Technical Report 496, 1935.

[7]   Sarkar, P. P., *New Identification Methods Applied to the Response of Flexible Bridges to Wind,* Ph.D. Dissertation, The John Hopkins University, Baltimore, MD, United States 1992.

[8]   Hafizh, H., *Identification of Flutter Derivatives of Bridge Deck from Wind Tunnel Test Data*, Master Thesis, Dept. of Aero-Astronautics, Institut Teknologi Bandung, Indonesia 2010.

[9]   Ibrahim, S. R., Mikulcik, E. C., *A Method for the Direct Identification of Vibration Parameters from the Free Response,* The Shock and Vibration Bulletin, Bulletin 47, Part 4, 1977.

[10] Gu, M., Zhang, R., Xiang, H., *Identification of Flutter Derivatives of Bridge Decks*, Journal of Wind Engineering and Industrial Aerodynamics, Vol. 84, pp. 151-162, 2000.

[11] Li, Y., Liao, H., Qiang, S., *Weighting Ensemble Least-Square Method for Flutter Derivatives of Bridge Decks*, Journal of Wind Engineering & Industrial Aerodynamics, Vol. 91, pp. 713-721, 2003.